https://doi.org/10.5194/egusphere-2026-1424
Preprint. Discussion started: 1 June 2026

Paleoclimate data assimilation with adaptive observation error inflation and adaptive localization

Ge Luo[1,2], Yuefei Zeng[1,2], Feng Zhu[3], and Jiuwei Zhao[1,2]

[1]State Key Laboratory of Climate System Prediction and Risk Management/Key Laboratory of Meteorological Disaster, Ministry of Education/Collaborative Innovation Center on Forecast and Evaluation of Meteorological Disasters, Nanjing University of Information Science and Technology, Nanjing 210044
[2]School of Atmospheric Sciences, Nanjing University of Information Science and Technology, Nanjing 210044
[3]Climate and Global Dynamics Laboratory, NSF National Center for Atmospheric Research, Boulder, CO, USA4

Correspondence: Yuefei Zeng (yuefei.zeng@nuist.edu.cn)

Abstract. Paleoclimate data assimilation methods significantly enhance the accuracy, spatiotemporal continuity, and global relevance of climate reconstructions by integrating Earth system models with proxy records. In this study, we further improve the algorithm by implementing two adaptive strategies—adaptive observation error inflation and adaptive localization—and systematically evaluate their performance in reconstructing temperature data over equatorial regions. For the adaptive observation error inflation experiments, two distinct methods were employed: the Adaptive observation error inflation (AOEI) method, which yields significant extreme improvements in specific regions but introduces notable local biases, and Huber Robust Estimation (HAOEI) method, which provides more robust and spatially consistent enhancement overall. In the adaptive localization experiments, observational density and correlation data were utilized to adjust the localization radius and weight matrix at each grid point. This approach effectively leverages sparse observational information, reduces spurious teleconnections, accurately reproduces the spatial structure of dominant climate variability modes, and optimizes the overall stability of the analyzed field.

1 Introduction

Reconstructing paleoclimate states is a crucial link in understanding the mechanisms and impacts of Earth system evolution. Currently, this field primarily relies on two methods: paleoclimate proxy records and Earth system model simulations. However, both approaches have significant limitations when reconstructing past climate states. On one hand, proxy records (such as tree rings, ice cores, speleothems, corals and etc.) play an indispensable role in reconstructing climate over the past millennia due to their long temporal span, but they often suffer from issues such as uneven spatiotemporal distribution, discontinuity, and sparsity. Furthermore, climate signals are easily contaminated by noise during preservation, making it extremely challenging to establish quantitative relationships between proxy indicators and the true climate state (Mann et al. 1998, 2008; Tingley et al. 2012; Liu et al. 2014; Guillot et al. 2015; Wang et al. 2015), and reconstructions of the same climate state from different proxy sources often show inconsistencies. On the other hand, climate models based on physical processes can provide physically consistent, globally complete climate fields with full spatiotemporal coverage, effectively capturing large-scale features of the climate system, however, due to inaccuracies in parameterizing physical processes and uncertainties in response to external

https://doi.org/10.5194/egusphere-2026-1424
Preprint. Discussion started: 1 June 2026

forcings, model simulations may exhibit systematic biases, struggling to fully reproduce observed climate variability and leading to limited predictive skills (Widmann et al. 2010; Phipps et al. 2013; Kageyama et al. 2021). Therefore, to overcome the limitations of individual methods, paleoclimate data assimilation (PDA) techniques have emerged as a powerful tool to optimally merge information from proxy records—sparse, noisy, and indirect indicators of past climate—with the dynamical constraints of climate models (Von Storch et al. 2000; Hakim et al. 2016; Goosse 2017). By doing so, the PDA method produces spatially complete and physically consistent climate field estimates, akin to reanalysis products for the instrumental era, while also quantifying reconstruction uncertainties. Among other methods, the Ensemble Kalman Filter (EnKF, Evensen (1994)), has gained prominence in PDA due to its easy implementation and capability to handle high-dimensional nonlinear systems (Hakim et al. 2016; Tardif et al. 2019; Osman et al. 2021; Sun et al. 2025).

Despite the great potential of PDA, it faces unique challenges distinct from modern meteorological data assimilation, primarily due to the fact that proxy records are fairly sparse in time and space, and often represent time-averaged climatic signals (e.g., annual means) rather than instantaneous observations. Furthermore, proxy data are subject to complex errors arising from measurement inaccuracies, chronological uncertainties, and the imperfect relationship between proxy signals and the target climate variables. In the PDA, observation error variance is often specified empirically from the residual variance of a Proxy System Model (PSM, Evans et al. (2013); Dee et al. (2015); Zhu et al. (2023)) calibrated against instrumental data. However, this method typically underestimates true proxy uncertainty, as it fails to account for calibration error (such as non-stationarity between past and instrumental periodes), structural error (arising from missing physics, biology, or chemistry in the PSM), and representation error (due to the mismatch between point-scale proxies and gridded state variables). To compensate, observation error inflation is frequently used (Sun et al. 2025). Given the strong spatial and temporal heterogeneity of proxy errors and information content, in PDA adaptive inflation methods are generally favored over a fixed inflation approach. While modern data assimilation has adopted techniques like Adaptive Observation Error Inflation (AOEI, Minamide and Zhang (2017)), its applicability to the specific challenges of the PDA remains insufficiently discussed and requires further exploration.

A critical factor for the success of the EnKF is its use of covariance localization. Early implementations typically employed a fixed localization radius (Houtekamer and Mitchell 1998, 2001). Within this framework, a common approach is to taper the sampled covariances—between observations and model states, or between different model states—using a smooth, distance-dependent function. A standard choice for this function is the Gaussian-like Gaspari-Cohn (GC) function (Gaspari and Cohn 1999). However, the Gaussian-like tapering function is not necessarily optimal as shown in several studies Anderson (2007); Lei and Anderson (2014a,b). To address limitations of the fixed localization, a range of adaptive localization methods have been developed. Those methods adjust the localization often in response to the state-dependent correlation patterns or ensemble-estimated errors. Examples include techniques developed by Anderson (2007, 2012), Bishop and Hodyss (2009a,b), and Ménétrier et al. (2015a,b). However, these methods have yet to be applied to PDA context. In PDA, a large covariance localization radius is typically employed due to the sparse distribution of proxy records (Tardif et al. 2019). While necessary, an excessively large localization radius can introduce spurious long-distance correlations, ultimately degrading analysis quality. This limitation suggests that localization with a fixed radius is suboptimal for PDA applications. Instead, an adaptive localization, which can optimize the influence radius of observations based on the underlying spatial correlation structures, applying

https://doi.org/10.5194/egusphere-2026-1424
Preprint. Discussion started: 1 June 2026

broader scales in regions with strong large-scale covariability and tighter constraints in data-rich or locally forced regions, is preferred. Currently, research on adaptive localization techniques in the PDA is still very limited.

In this paper, adaptive observation error inflation and adaptive covariance localization will be developed and explored within an ensemble-based PDA framework, aiming to create a more flexible and accurate assimilation system. As a methodological paper, a pseudoproxy experiment might be more informative than a real-word one. But we directly conduct real-world proxy experiments using a climate model to systematically evaluate whether these adaptive strategies can enhance reconstruction skill—particularly in sparse data regimes—improve uncertainty quantification, and provide a more generalizable approach for assimilating the heterogeneous and uncertain proxy records that characterize paleoclimatology.

2 Methods

2.1 Adaptive observation error inflation

The AOEI was first introduced and systematically applied in the context of satellite radiance data assimilation for numerical weather prediction (Minamide and Zhang 2017). It operates as in Eq. (1) by inflating the observation error variance when the squared innovation — the difference between the observation and the model simulation — exceeds the ensemble spread of the model simulation:

$$\mathbf{R} = \max\left\{\sigma_{\mathrm{ot}}^2, \left[\mathbf{y} - H(\overline{\mathbf{x}}_f)\right]^2 - \sigma_{H(\mathbf{x})}^2\right\}, \tag{1}$$

where σ_{ot}^2 is the uninflated observation error variance, $\mathbf{y} - H(\overline{\mathbf{x}}_f)$ is the innovation, and $\sigma_{H(\mathbf{x})}^2$ is the ensemble spread in observation space.

The AOEI is designed to limit erroneous analysis increments where there are large representativeness errors in either the forecast model and/or from the observation itself. However, its aggressive adjustment strategy (inflation grows with the square of innovation) requires careful application in data-sparse regions or areas with uncertain observations to avoid amplifying noise.

2.2 Huber Robust Estimation

In this study, a new adaptive observation error inflation scheme based on the Huber robust estimation method (Huber 1992) is introduced (hereafter called "HAOEI"), which aims to mitigate the undue influence of large outliers. This method computes a normalized innovation—the difference between the observation and the model forecast, normalized by the square root of the sum of the model forecast error variance and the baseline observational error variance—and compares it against a threshold δ. The baseline observational error variance is then inflated for values exceeding this threshold. The simplified formulation is as follows:

$$r = \frac{\mathbf{y} - H(\overline{\mathbf{x}}_f)}{\sqrt{\sigma_{H(\mathbf{x})}^2 + \sigma_{\mathrm{ot}}^2}}, \tag{2}$$

https://doi.org/10.5194/egusphere-2026-1424
Preprint. Discussion started: 1 June 2026

$$R = \begin{cases} \sigma_{\mathrm{ot}}^2, & \text{for } |r| \le \delta, \\ \sigma_{\mathrm{ot}}^2 \cdot \frac{|r|}{\delta}, & \text{for } |r| > \delta. \end{cases} \tag{3}$$

The threshold parameter δ defines the boundary between normal observations and potential outliers, typically chosen based on statistical significance levels (e.g., $\delta \approx 1.645$ corresponds to the 90% confidence interval of a standard normal distribution). Observations with normalized innovations within $\pm\delta$ are considered statistically consistent with the forecast and retain their original error variance, while those beyond this range are treated as potential outliers and undergo error variance inflation.

It is noted that the AOEI amplifies observation error variance in proportion to the square of the innovation and acts as a high-sensitivity tool. It can produce substantial localized corrections where the model and a proxy strongly disagree, but its aggressive response also risks misclassifying accurate observations as outliers, thereby introducing new regional biases. Conversely, the HAOEI applies a more moderated, linear inflation only when the normalized innovation surpasses a defined threshold. This design makes it a robust stabilizer; it consistently improves performance across wider areas by avoiding extreme adjustments, though it may not achieve the same level of peak correction in the most severely mismatched locations.

2.3 Adaptive localization

Due to the uneven spatial distribution of proxy data, localization is required to constrain their spurious influence on remote regions. Within a fixed localization radius PDA framework, a weight matrix was introduced by Tardif et al. (2019) to adjust the covariance. This weight matrix is defined by the Gaspari–Cohn function (Gaspari and Cohn 1999):

$$w_{ij} = \mathrm{GC}(d_{ij}, L) \tag{4}$$

where w_{ij} is the weight assigned to observation $\mathbf{x}_j$ when updating grid point $\mathbf{x}_i$, d_{ij} is the distance between grid point and observation, L is a specified cut-off (or localization) radius, and GC denotes the Gaspari–Cohn fifth-order polynomial:

$$\mathrm{GC}(z_{ij}) = \begin{cases} 1 - \frac{5}{3}z_{ij}^2 + \frac{5}{8}z_{ij}^3 + \frac{1}{2}z_{ij}^4 - \frac{1}{4}z_{ij}^5, & 0 \le z_{ij} \le 1 \\ -\frac{2}{3}z_{ij}^{-1} + 4 - 5z_{ij} + \frac{5}{3}z_{ij}^2 + \frac{5}{8}z_{ij}^3 - \frac{1}{2}z_{ij}^4 + \frac{1}{12}z_{ij}^5, & 1 < z_{ij} \le 2 \\ 0, & z_{ij} > 2 \end{cases} \tag{5}$$

where $z_{ij} = \frac{d_{ij}}{L/2}$.

While effective in many contexts, this method typically requires a relatively large, uniform localization radius to compensate for sparse data coverage and considers only physical distance, ignoring spatially varying data density and potential teleconnections. To address these limitations, we introduce an adaptive localization scheme that determines more appropriate localization radii for each model grid point based on local observational density. The core idea is to assign a larger radius in data-sparse regions to draw in more information and a smaller radius in data-dense regions to reduce unnecessary smoothing and computational cost.

https://doi.org/10.5194/egusphere-2026-1424
Preprint. Discussion started: 1 June 2026

Observational density is estimated at each grid point using kernel density estimation (KDE) with a Gaussian kernel (Parzen 1962). For a given grid point $\mathbf{x}_i$, the density is computed as:

$$\rho^*(\mathbf{x}_i) = \frac{1}{nh^2} \sum_{j=1}^{n} K\left(\frac{\|\mathbf{x}_i - \mathbf{o}_j\|}{h}\right) \tag{6}$$

where n is the total number of proxy observations, $\mathbf{o}_j$ denotes the location of the j-th observation, h is the bandwidth parameter, and $K(\cdot)$ is the Gaussian kernel function:

$$K(u) = \frac{1}{2\pi} e^{-\frac{u^2}{2}}. \tag{7}$$

The bandwidth h is determined using Scott's rule:

$$h = n^{-1/6} \cdot \hat{\sigma}, \tag{8}$$

where $\hat{\sigma}$ is the standard deviation between observation locations. This choice provides a data-adaptive smoothing that balances bias and variance in density estimation, yielding a continuous density field. This density field is then normalized by its global maximum value to obtain $\rho(\mathbf{x}_i) \in [0, 1]$, representing the relative data density at grid point $\mathbf{x}_i$. Based on this, the localization radius $L(\mathbf{x}_i)$ at grid point $\mathbf{x}_i$ is defined as a function of this normalized density.

$$L(\mathbf{x}_i) = \begin{cases} L \cdot \left(1 - \rho(\mathbf{x}_i)^{1/2}\right), & \text{if } L \cdot \left(1 - \rho(\mathbf{x}_i)^{1/2}\right) \geq L_{\text{min}} \\ L_{\text{min}}, & \text{otherwise} \end{cases} \tag{9}$$

where L is the original fixed localization radius (attained in observation-sparse regions where $\rho(\mathbf{x}_i) \to 0$), the exponent $1/2$ controls the curvature of the density-to-radius mapping, and L_{min} is a lower bound enforced to maintain a minimum influence range even in observation-dense regions.

However, adjusting the localization radius solely based on density may further reduce the number of effective observations available for some grid points. While this helps suppress spurious teleconnections, it can also limit the use of already sparse paleoclimate proxy data, potentially undermining assimilation performance.

To better balance the use of observational information and the suppression of spurious correlations, we further incorporate correlation information into the weighting strategy, i.e., for observations outside the localization radius, their influence weight depends on the correlation ($w_{ij} \sim corr$). The correlation coefficient r_{ij} between grid point $\mathbf{x}_i$ and observation $\mathbf{x}_j$ is computed as the Pearson correlation coefficient between their respective time series over the reconstruction period:

$$r_{ij} = \frac{\sum_{t=1}^{T} (\mathbf{x}_{i,t} - \bar{\mathbf{x}}_i)(\mathbf{y}_{j,t} - \bar{\mathbf{y}}_j)}{\sqrt{\sum_{t=1}^{T} (\mathbf{x}_{i,t} - \bar{\mathbf{x}}_i)^2 \sum_{t=1}^{T} (\mathbf{y}_{j,t} - \bar{\mathbf{y}}_j)^2}}, \tag{10}$$

where $\mathbf{x}_{i,t}$ is the value at grid point $\mathbf{x}_i$ at time t, $\mathbf{y}_{j,t}$ is the value at observation $\mathbf{x}_j$ at time t, $\bar{\mathbf{x}}_i$ and $\bar{\mathbf{y}}_j$ are the temporal means of the respective series, and T is the length of the time series. This coefficient quantifies the statistical relationship between distant locations and helps identify teleconnections that are physically meaningful rather than spurious.

https://doi.org/10.5194/egusphere-2026-1424
Preprint. Discussion started: 1 June 2026

The final weight w_{ij} assigned to observation $\mathbf{x}_j$ when updating grid point $\mathbf{x}_i$ is then defined as a hybrid of distance-based and correlation-based weighting:

$$w_{ij} = \begin{cases} \frac{1}{2} \cdot |r_{ij}|, & \text{if } d_{ij} > L_i \text{ and } |r_{ij}| > 0.2 \\ \mathrm{GC}(d_{ij}, L_i), & \text{else} \end{cases} \tag{11}$$

where d_{ij} is the distance between grid point $\mathbf{x}_i$ and observation $\mathbf{x}_j$, $L_i = L(\mathbf{x}_i)$ is the adaptive localization radius at grid point $\mathbf{x}_i$ computed from Eq. (9), $r_{ij} \in [-1, 1]$ is the correlation coefficient, 0.2 is the set expression threshold. This hybrid strategy maintains the stability of distance-based localization within the adaptive radius while selectively incorporating influential remote observations based on statistical correlation, thereby improving the assimilation of sparse proxy data without amplifying spurious teleconnections.

3 Experimental design and results

3.1 Experimental design

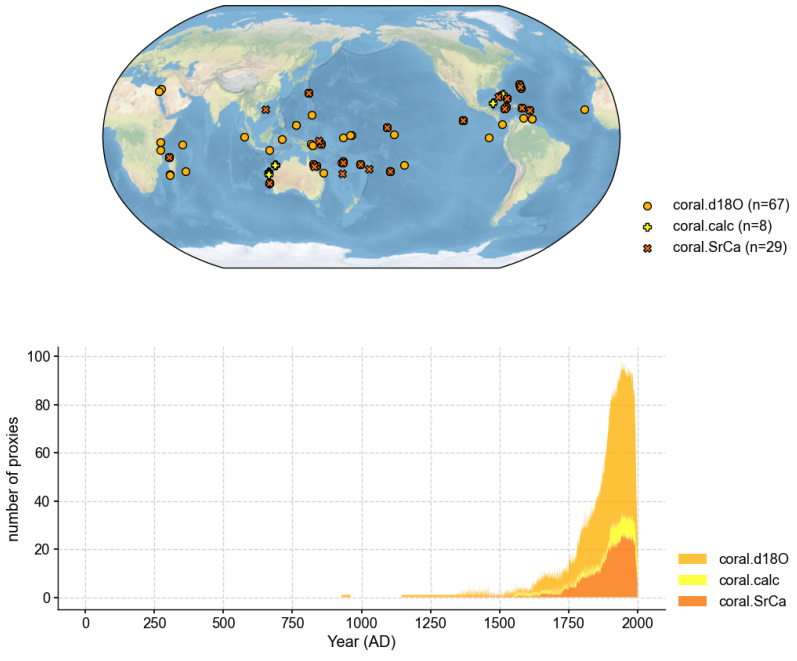

Figure 1. Spatial and temporal distributions of proxy records from the PAGES 2k dataset, visualized with cfr (Zhu et al. 2024)

To evaluate the effectiveness of adaptive inflation and adaptive localization methods, a set of sensitivity experiments (Table 1) is conducted using the cfr framework (v2024.1.26, Zhu et al. (2024)). The goal is to reconstruct tropical (30°S–30°N)

https://doi.org/10.5194/egusphere-2026-1424
Preprint. Discussion started: 1 June 2026

Table 1. Experimental setups, which are divided into two groups, sensitivity experiments on observation error inflation and on localization.

Group	EXP	Localization	Observation error inflation	Estimation of correlations in Eq. (10)
Adaptive observation error inflation				
	E_20000	20,000 km	No	–
	E_AOEI	20,000 km	AOEI	–
	E_HAOEI0.67	20,000 km	HAOEI, $\delta = 0.67$	–
	E_HAOEI1.04	20,000 km	HAOEI, $\delta = 1.04$	–
Adaptive localization				
	E_20000	20,000 km	No	–
	E_10000	10,000 km	No	–
	E_5000	5,000 km	No	–
	E_1000	1,000 km	No	–
	E_AL1	(Adaptive)	No	Reanalyses
	E_AL2	(Adaptive)	No	Model priors
	E_HAOEI0.67_AL1	(Adaptive)	HAOEI, $\delta = 0.67$	Reanalyses
	E_HAOEI0.67_AL2	(Adaptive)	HAOEI, $\delta = 0.67$	Model priors

surface temperature anomalies from 1880 to 2000, with respect to the 1951–1980 climatological baseline. The prior ensemble is drawn from the "iCESM1" last millennium and historical simulations (Brady et al. 2019), which provide physically consistent climate backgrounds spanning 850–2000 CE. Coral-based proxy records from the PAGES 2k Phase 2 database (PAGES 2k Consortium 2017)—calibrated against NASA GISTEMP v4 (Lenssen et al. 2019)—are assimilated. These records are selected due to their strong temperature sensitivity and predominant distribution within the tropics (Figure 1). Focusing on the tropics is motivated by two main reasons: first, the high temperature sensitivity of coral proxies enhances reconstruction reliability, whereas incorporating other proxy types (e.g., tree rings, ice cores) at a global scale could increase uncertainty due to their generally lower temperature sensitivity. Second, the tropics contain key climate systems such as ENSO, frequently studied in paleoclimatology, allowing for a clear assessment of methodological performance while reducing computational costs. It is important to note that the methodology presented here can, in principle, be extended to global applications. In the following, the impact of adaptive observation error is first assessed by comparing two inflation schemes—AOEI and HAOEI. Next, sensitivity experiments investigate the role of localization. Initial tests use fixed localization radii, which are then compared to two experiments employing the adaptive localization method described in Section 2.3—one estimating proxy–state correlations based ob reanalysis data GISTEMP v4, and the other one based on the model priors from "ICESM1" last millennium simulations. All data assimilation experiments cover 1880–2000, use a one-year assimilation window, and an ensemble size of 100.

https://doi.org/10.5194/egusphere-2026-1424
Preprint. Discussion started: 1 June 2026

Three metrics are computed to evaluate the reconstruction analyses: the Root Mean Square Error (RMSE), the Coefficient of Efficiency (CE), and the Empirical Orthogonal Function (EOF). The RMSE for a given model grid point q is defined as:

$$\mathrm{RMSE}(q) = \sqrt{\frac{1}{n}\sum_{t=1}^{n}(\mathbf{v}_{q,t} - \overline{\mathbf{x}}_{q,t})^2}, \tag{12}$$

where n is the number of time samples, $\mathbf{v}_{q,t}$ is the verification data at grid point q and time t, and $\overline{\mathbf{x}}_{q,t}$ is the corresponding prior or posterior ensemble mean.

The CE evaluates the skill of the reconstruction relative to the climatological mean of the verification data. For a given model grid point q, it is calculated as:

$$\mathrm{CE}(q) = 1 - \frac{\sum_{t=1}^{n}(\mathbf{v}_{q,t} - \overline{\mathbf{x}}_{q,t})^2}{\sum_{t=1}^{n}(\mathbf{v}_{q,t} - \overline{\mathbf{v}}_{q})^2}, \tag{13}$$

where $\overline{\mathbf{v}}_q$ is the temporal mean of the verification data at grid point q. A CE value close to 1.0 indicates a highly accurate reconstruction, a value of 0 means the reconstruction is only as accurate as the climatological mean, and negative values suggest lower skill.

Beyond pointwise accuracy metrics, we also examine the ability of the reconstructions to capture the dominant large-scale modes of climate variability. For this purpose, we apply Empirical Orthogonal Function (EOF) analysis (Lorenz et al. 1956) to the reconstructed spatial fields The EOF method decomposes a spatiotemporal field $\mathbf{X}(s,t)$ into a set of orthogonal spatial patterns (EOFs) and their associated principal component (PC) time series. The leading EOF mode explains the largest possible fraction of the total variance, with each subsequent mode explaining the maximum remaining variance under the constraint of orthogonality to all previous modes. The corresponding PCs represent the temporal evolution of these spatial patterns. In the following analysis, we compare the leading EOF modes—their spatial patterns, explained variance—obtained from different reconstruction methods against those derived from the verification dataset, to assess which method better recovers the key climate teleconnections and oscillatory signals.

As validation data, The spatially completed version of the near-surface air temperature and sea-surface temperature analyses product HadCRUT4.6 (Vaccaro et al. 2021) is employed.

3.2 Results

3.2.1 Adaptive observation error inflation

Figure 2 shows the RMSE for the surface temperature analyses in experiment E_20000, as well as the RMSE differences between E_20000 and E_AOEI, E_HAOEI(0.67) and E_HAOEI(1.04). The largest RMSE values in E_20000 are located in the equatorial ENSO region. E_AOEI produces a noticeable reduction in RMSE (mean difference = –0.0195 °C) relative to E_20000. This improvement stems primarily from its aggressive error-inflation strategy, which strongly down-weights observations that deviate sharply from the model prior—most effectively in regions such as the ENSO zone where model biases are large. However, the same mechanism can also suppress accurate observations where the prior is poor, leading to local error

https://doi.org/10.5194/egusphere-2026-1424
Preprint. Discussion started: 1 June 2026

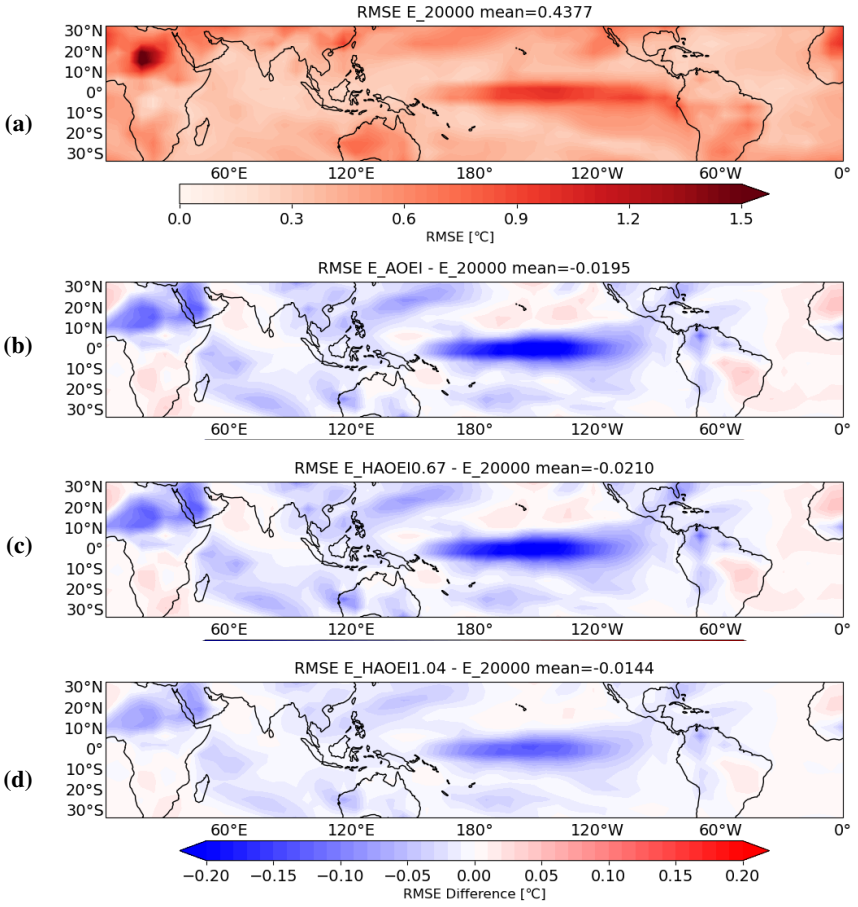

Figure 2. (a) the RMSE for the surface temperature analyses in E_20000 (b) the RMSE differences between E_AOEI and E_20000 (c) between E_HAOEI(0.67) and E_20000 and (d) between E_HAOEI(1.04) and E_20000

increases, as seen over the North Pacific and Atlantic. The HAOEI apply a more moderate, threshold-dependent inflation. With a higher threshold (δ = 1.04), E_HAOEI(1.04) yields widespread but modest improvements and fewer areas of degradation, resulting in a mean RMSE difference of –0.0144 °C. A lower threshold (δ = 0.67) in E_HAOEI(0.67) strikes a more effective balance, delivering stronger overall error reduction (mean difference = –0.0210 °C) and outperforming both E_AOEI and E_HAOEI(1.04). Similar performance patterns are reflected in the CE (Figure 3). While E_AOEI yields considerably higher CE values than E_20000, tuning δ can adjust the skill, with E_HAOEI(0.67) achieving superior performance to E_AOEI.

Figure 4 compares the spatial pattern and PC time series of the leading EOF mode derived from the observations with those from the reconstructed analyses of E_AOEI, E_HAOEI($\delta = 0.67$) and E_HAOEI($\delta = 1.04$). All experiments display a similar spatial structure to the observations, yet they show markedly stronger variability in the ENSO region and produce a substantially higher explained variance. This discrepancy suggests that within the current assimilation framework, the reconstructed temperature field may be overly focused on a single dominant spatial mode, thereby failing to capture the more dispersed,

https://doi.org/10.5194/egusphere-2026-1424
Preprint. Discussion started: 1 June 2026

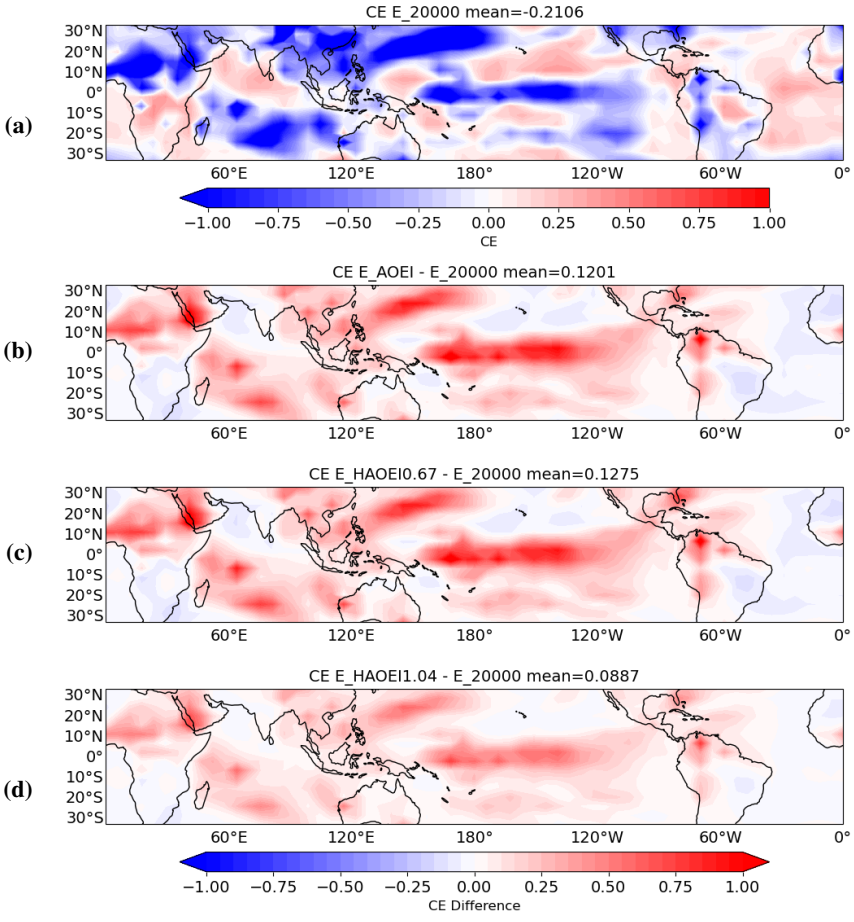

Figure 3. Same as Figure 2 but for the CE

multi-scale variability present in the actual observations. This effect may be partly due to the use of an excessively large localization radius, a point that will be further discussed in the following section.

3.2.2 Adaptive localization

Figure 5 presents the time series of RMSE for surface temperature analyses across experiments using different fixed localization radii (1000–20000 km). Except extremely small localization radius of 1000 km, the RMSE generally increases as the localization radius grows, which is consistent with other studies (e.g., Zeng and Janjić (2016)): too small radius ignores physical correlations and introduces unbalanced structures; too larger radius allows spurious correlations to persist over the domain and thus an observation incorrectly influences states that are physically unrelated to it. Furthermore, regarding the leading EOF mode as shown in Figure 6, while smaller radii yield explained variance values closer to those of the observations, they also significantly distort the spatial pattern of variability. In summary, although smaller localization radii tend to reduce RMSE

https://doi.org/10.5194/egusphere-2026-1424
Preprint. Discussion started: 1 June 2026

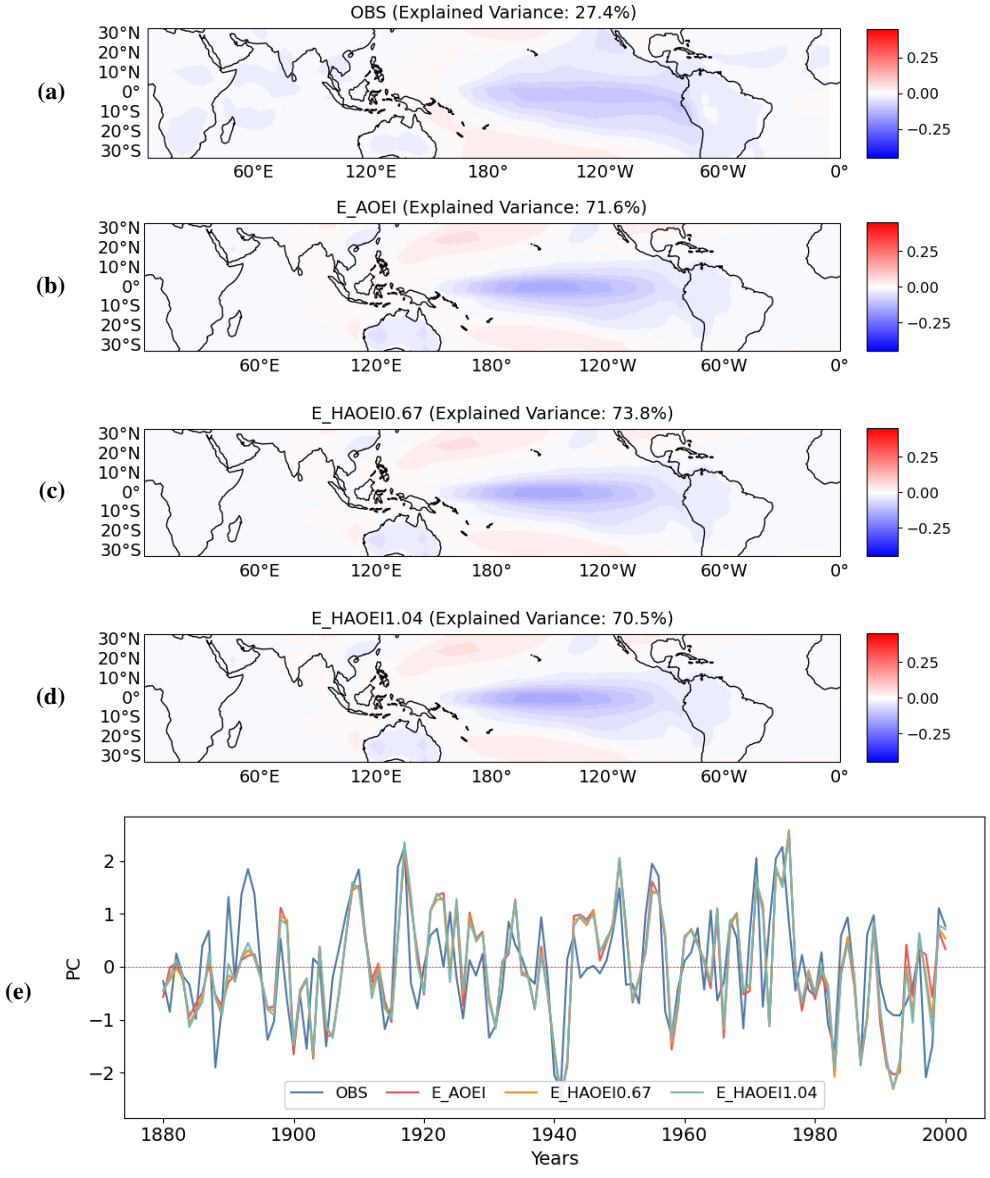

Figure 4. The leading EOF mode of (a) observations (b) E_AOEI analyses (c) E_HAOEI ($\delta = 0.67$) analyses (d) E_HAOEI ($\delta = 1.04$) analyses (e) corresponding PC time series for all experiments

and preserve fine-scale variability, they can also degrade the representation of coherent, large-scale variability structures. This trade-off highlights the need for an adaptive localization approach that can balance these competing objectives.

To implement the adaptive localization method described in Section 2.3, the spatial density of proxy records is first estimated using kernel density estimation (KDE), as visualized in Figure 7. While this density varies from year to year, the time-averaged distribution reveals distinct regional patterns: Australia and Central America are data-rich, the equatorial ENSO region exhibits

https://doi.org/10.5194/egusphere-2026-1424
Preprint. Discussion started: 1 June 2026

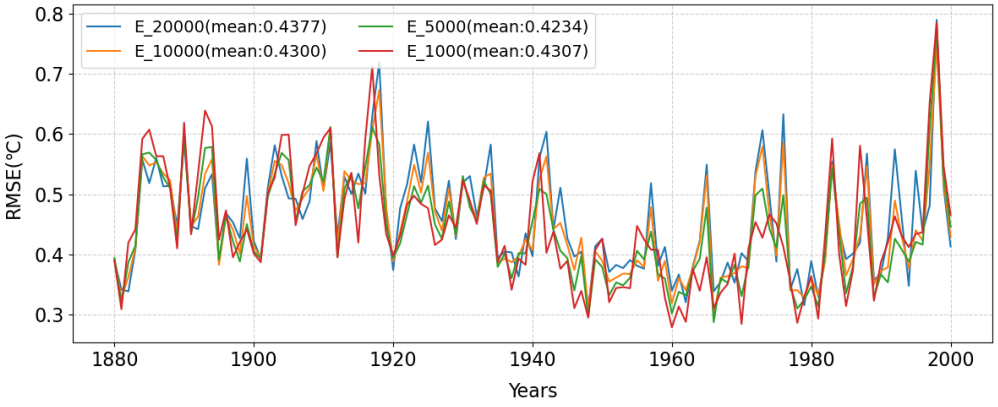

Figure 5. The time series of the RMSE for the surface temperature analyses in experiments with varying fixed localization radii

medium proxy density, and areas such as South America remain relatively data-sparse. Furthermore, proxy-state correlations given in Eq. 10 are given by using the reanalyses and model priors, respectively. Figure 8 illustrates the correlations for one representative proxy record (ID: Ocn_090). Both estimated correlations reflect similar spatial structures but with detailed differences, e.g., the former one shows generally higher values and distinct discrepancies over Africa and the adjacent Indian Ocean region.

As shown in Figure 9 and Figure 10, E_AL1 outperforms E_20000, yielding smaller RMSEs and generally higher CEs. The improvements scale with data density: moderate in data-rich regions (e.g., Australia, Central America), more substantial in medium-density areas like the equatorial ENSO region, and largely neutral in sparse-data regions such as South America. Similarly, E_HAOEI0.67 achieves slightly lower RMSEs and higher CEs than its adaptive-localization counterpart, E_HAOEI0.67_AL1. Furthermore, Figure 11 reveals that the leading EOF modes of E_AL1 and E_HAOEI0.67_AL1 exhibit a spatial structure similar to observations but with amplified variability in the ENSO region. Although their explained variance remains substantially higher than observed, it is considerably lower than that of E_20000 (Figure 6). Overall, the application of adaptive localization is beneficial for enhancing reconstruction quality, both in terms of statistical accuracy and the fidelity of dominant climate modes.

Finally, Figure 12 illustrates that adaptive localization using model-prior correlations E_AL2 improves upon the fixed-radius baseline E_20000, as evidenced by its lower RMSEs and higher CEs, even if it does not match the performance of the reanalysis-driven version E_AL1. This demonstrates the intrinsic value of the model prior: its physically constrained correlations offer a viable and effective guide for adaptive localization in the absence of reanalysis data. Consequently, this approach ensures the method's applicability to pre-industrial and deeper-time paleoclimate periods, where observational constraints are otherwise unavailable.

https://doi.org/10.5194/egusphere-2026-1424
Preprint. Discussion started: 1 June 2026

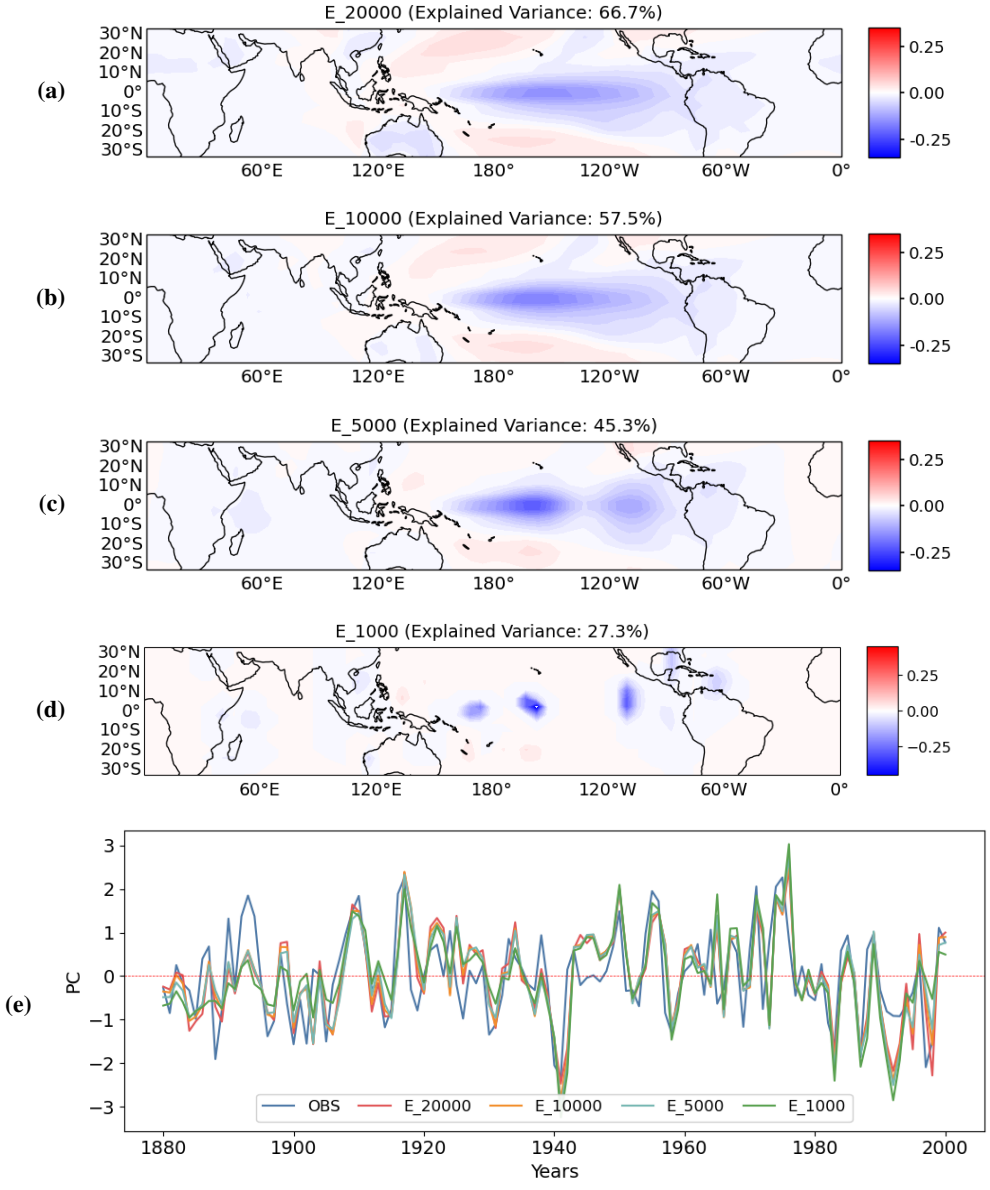

Figure 6. The leading EOF mode of the tropics: (a) Reconstructed EOF field with 20,000 km localization radius; (b) Reconstructed EOF field with 10,000 km localization radius; (c) Reconstructed EOF field with 5,000 km localization radius; (d) Reconstructed EOF field with 1,000 km localization radius; (e) Corresponding principal component (PC) time series for all experiments. All results are based on the period 1880–2000. EOF units are °C.

https://doi.org/10.5194/egusphere-2026-1424
Preprint. Discussion started: 1 June 2026

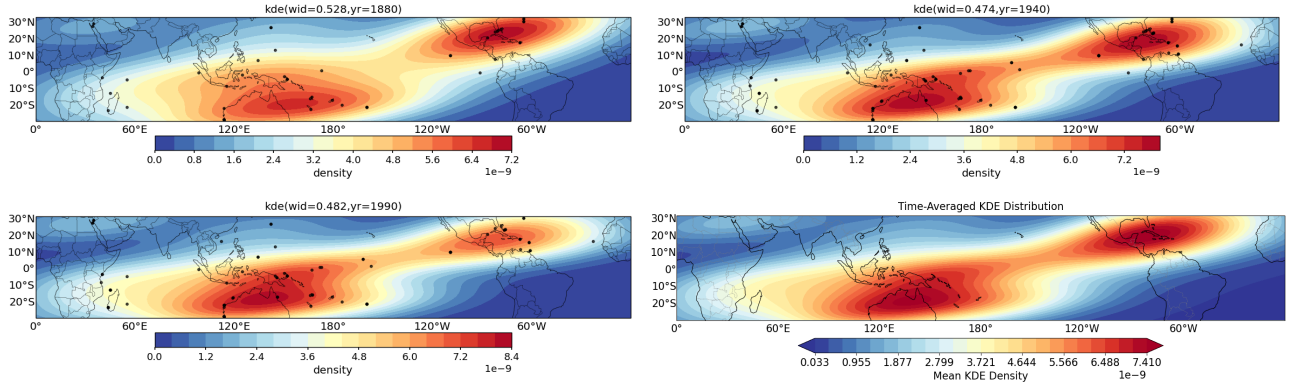

Figure 7. Gaussian kernel density estimation maps for different years: (a) 1880; (b) 1940; (c) 1990; (d) time averaged

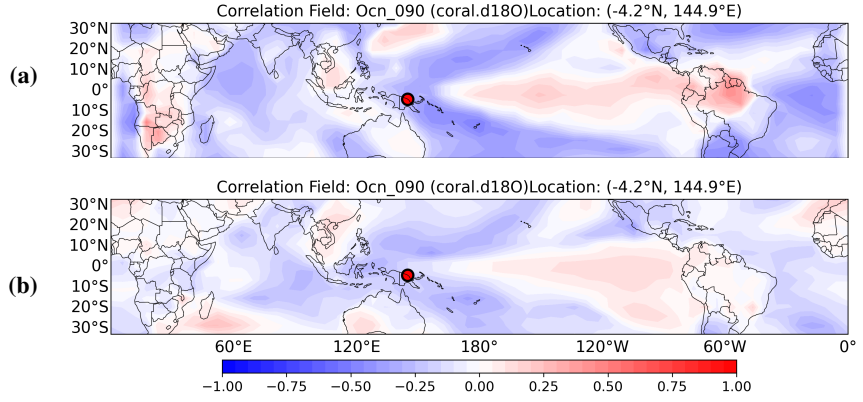

Figure 8. Spatial correlation maps between coral proxy data (ID: Ocn_090) located at 4.2°S, 144°E and (top) instrumental observations, (bottom) prior data.All experiments are based on the period 1880-2000

4 Conclusion and outlook

This study develops and evaluates adaptive data assimilation strategies specifically designed to address the challenges inherent in the PDA. Two adaptive observation error inflation methods are introduced and compared and a novel adaptive localization scheme is proposed within an ensemble-based PDA framework of cfr. The adaptive observation error inflation technique improves reconstruction accuracy by dynamically adjusting observation uncertainties. While the aggressive AOEI method yields significant error reductions in regions with strong model-data mismatch, such as the equatorial ENSO zone, it risks introducing local biases by disproportionately inflating errors for accurate observations. In contrast, the Huber-based adaptive scheme (HAOEI) delivers more balanced and robust performance. With an optimally tuned threshold, HAOEI achieves the strongest overall reduction in RMSEs and increase in CEs, outperforming both the baseline and the AOEI approach. Furthermore, the developed adaptive localization scheme effectively mitigates the limitations of fixed-radius localization in the context of sparse

https://doi.org/10.5194/egusphere-2026-1424
Preprint. Discussion started: 1 June 2026

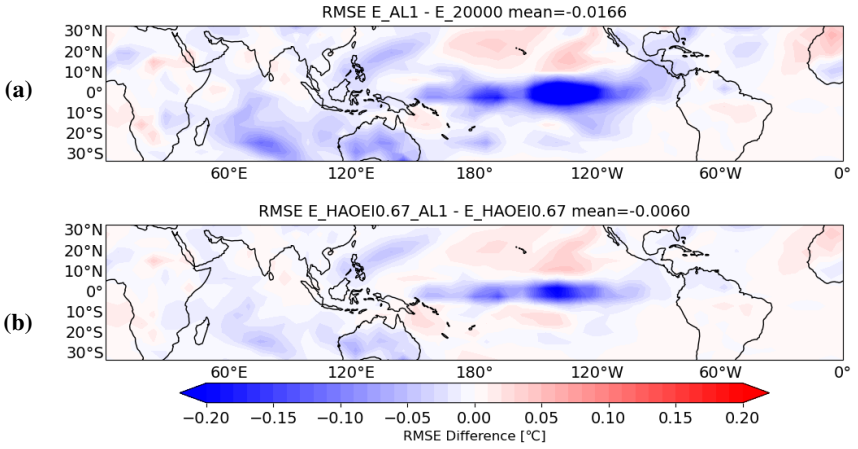

Figure 9. (a) the RMSE differences between E_AL1 and E_20000 (b) between E_HAOEI0.67_AL1 and E_HAOEI0.67

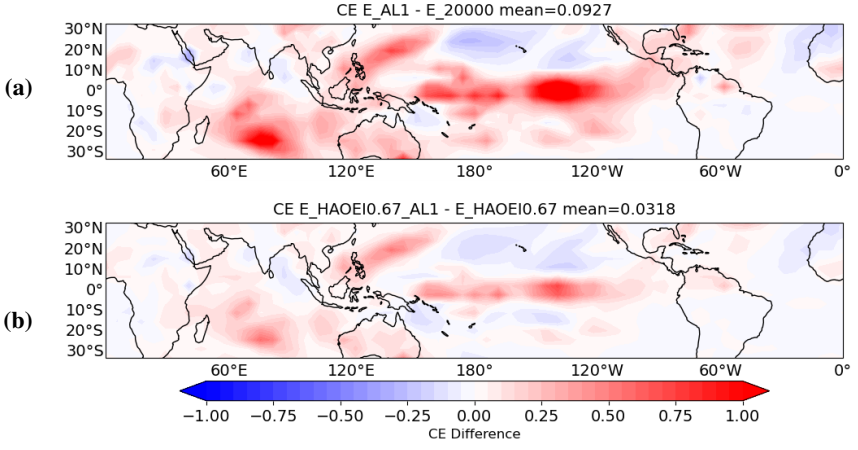

Figure 10. Same as Figure 9 but for the CE

and unevenly distributed proxy data. By dynamically adjusting the localization radius according to local observational density and selectively incorporating correlation-based weights, the method enhances the utilization of available proxy information while suppressing spurious long-range correlations. Compared to experiments employing a large fixed radius, the adaptive configuration yields lower RMSEs and higher CEs, with the most substantial improvements occurring in regions of medium data density, such as the equatorial ENSO region. Regarding the fidelity of spatial climate modes, while all assimilation experiments tend to amplify ENSO-related variability and overestimate the explained variance of the leading EOF mode, the adaptive localization produces spatial patterns that more closely align with observations. Notably, it substantially reduces the inflated explained variance characteristic of large fixed-radius localization, indicating a more skillful balance between capturing large-scale coherence and preserving realistic variance distribution.Importantly, the adaptive method remains effective even when

https://doi.org/10.5194/egusphere-2026-1424
Preprint. Discussion started: 1 June 2026

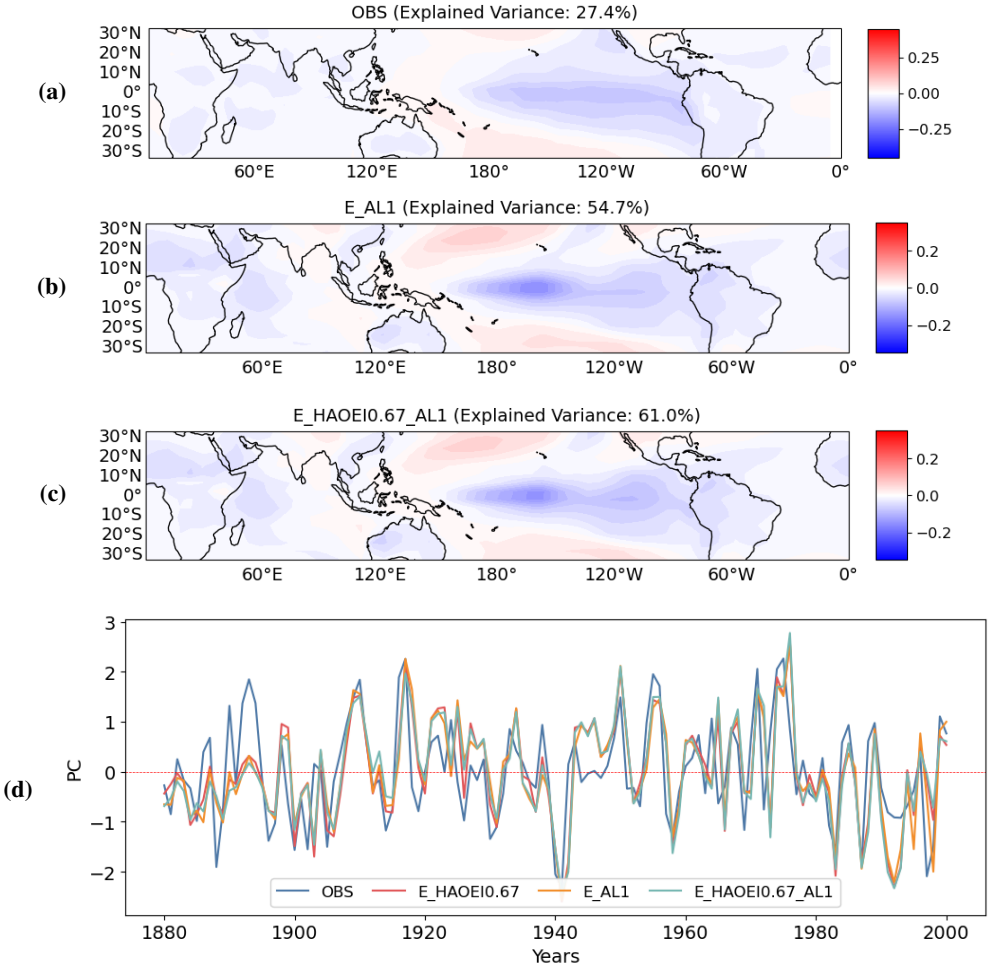

Figure 11. The leading EOF mode of (a) observations (b) adaptive localization analyses (c) adaptive localization and HAOEI ($\delta = 0.67$) analyses (d) corresponding PC time series for all experiments

correlation information is derived solely from the model prior, extending its applicability to pre-instrumental periods where reanalysis data are unavailable. Collectively, these adaptive methodologies contribute to more accurate, reliable, and physically consistent reconstructions of past climate variability.

While this study demonstrates the considerable promise of adaptive strategies in paleoclimate data assimilation, several important avenues merit further investigation to advance the methodology and expand its applications. This study focused on coral-based temperature reconstructions within the tropics; extending the framework to a global scale and to multiple proxy types and climate variables would provide a rigorous test of its generalizability and enable more holistic climate field reconstructions. The methods should be also tested during periods of abrupt climate change (e.g., the Last Glacial Termination, Dansgaard–Oeschger events) or past warm periods (e.g., the Last Interglacial, the Pliocene), where data constraints are particularly challenging but scientific stakes are high.

https://doi.org/10.5194/egusphere-2026-1424
Preprint. Discussion started: 1 June 2026

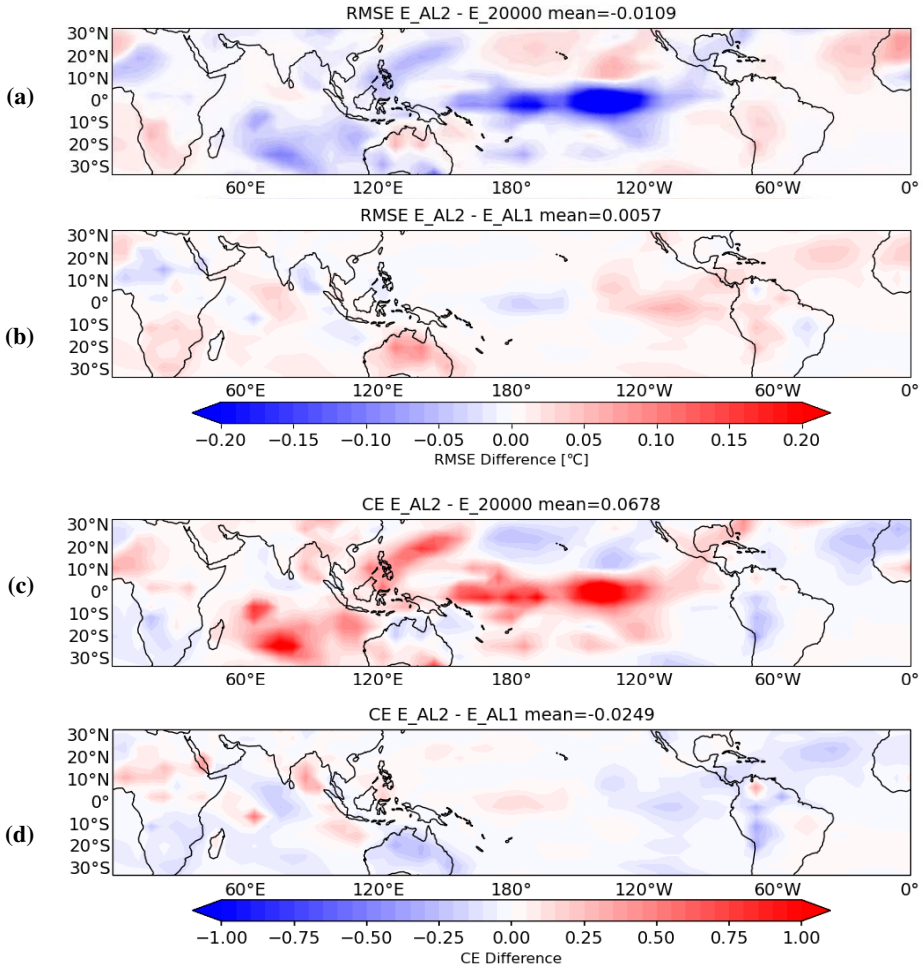

Figure 12. (a) the RMSE differences between E_AL2 and E_20000 (b) between E_AL2 and E_AL1 (c) the CE differences between E_AL2 and E_20000 (d) between E_AL2 and E_AL1

Code and data availability. The code and data that support the findings of this study are openly available. All input datasets actually used in this study (including the PAGES 2k Phase 2 global multiproxy database, the "iCESM1" last millennium simulation, the NASA Goddard's Global Surface Temperature Analysis, as well as the spatially completed version of the near-surface air temperature and sea-surface temperature analysis product HadCRUT4.6) are hosted within the cfr and can be accessed at: https://zenodo.org/record/10575537. The exact version of the code, the source code of the assimilation system, and the validation results of the reconstructed estimates used in this study are also archived in a trusted permanent repository at Zenodo under the following DOI: https://doi.org/10.5281/zenodo.19015635 (Luo et al. 2026).

https://doi.org/10.5194/egusphere-2026-1424
Preprint. Discussion started: 1 June 2026

Author contributions. G. Luo conducted the experiments and wrote the first draft of the manuscript. Y. Zeng and F. Zhu proposed the ideas of adaptive observation error inflation and adaptive localization, and implemented them. J. Zhao contributed to the analysis of the results. All authors contributed to revising the text and defining the structure of the paper.

Competing interests. The authors have the following competing interests: one coauthor is a member of the editorial board of Geoscientific Model Development

Acknowledgements. We acknowledge financial support from the National Key Research and Development Program of China

Financial support. National Key Research and Development Program of China (grant no. 2023YFF0804703).

https://doi.org/10.5194/egusphere-2026-1424
Preprint. Discussion started: 1 June 2026

References

Anderson, J. L.: Exploring the need for localization in ensemble data assimilation using a hierarchical ensemble filter, Physica D: Nonlinear Phenomena, 230, 99–111, 2007.

Anderson, J. L.: Localization and sampling error correction in ensemble Kalman filter data assimilation, Monthly Weather Review, 140, 2359–2371, 2012.

Bishop, C. and Hodyss, D.: Ensemble covariances adaptively localized with ECO-RAP. Part 1: Tests on simple error models, Tellus A: Dynamic Meteorology and Oceanography, 61, 84–96, 2009a.

Bishop, C. and Hodyss, D.: Ensemble covariances adaptively localized with ECO-RAP. Part 2: A strategy for the atmosphere, Tellus A: Dynamic Meteorology and Oceanography, 61, 97–111, 2009b.

Brady, E., Stevenson, S., Bailey, D., Liu, Z., Noone, D., Nusbaumer, J., Otto-Bliesner, B. L., Tabor, C., Tomas, R., Wong, T., et al.: The connected isotopic water cycle in the Community Earth System Model version 1, Journal of Advances in Modeling Earth Systems, 11, 2547–2566, 2019.

Dee, S., Emile-Geay, J., Evans, M., Allam, A., Steig, E., and Thompson, D.: PRYSM: An open-source framework for PRoxY System Modeling, with applications to oxygen-isotope systems, Journal of Advances in Modeling Earth Systems, 7, 1220–1247, 2015.

Evans, M. N., Tolwinski-Ward, S. E., Thompson, D. M., and Anchukaitis, K. J.: Applications of proxy system modeling in high resolution paleoclimatology, Quaternary science reviews, 76, 16–28, 2013.

Evensen, G.: Sequential data assimilation with a nonlinear quasi-geostrophic model using Monte Carlo methods to forecast error statistics, Journal of Geophysical Research: Oceans, 99, 10 143–10 162, 1994.

Gaspari, G. and Cohn, S. E.: Construction of correlation functions in two and three dimensions, Quarterly Journal of the Royal Meteorological Society, 125, 723–757, 1999.

Goosse, H.: Reconstructed and simulated temperature asymmetry between continents in both hemispheres over the last centuries, Climate Dynamics, 48, 1483–1501, 2017.

Guillot, D., Rajaratnam, B., and Emile-Geay, J.: Statistical paleoclimate reconstructions via Markov random fields, The Annals of Applied Statistics, 9, 324–352, 2015.

Hakim, G. J., Emile-Geay, J., Steig, E. J., Noone, D., Anderson, D. M., Tardif, R., Steiger, N., and Perkins, W. A.: The last millennium climate reanalysis project: Framework and first results, Journal of Geophysical Research: Atmospheres, 121, 6745–6764, 2016.

Houtekamer, P. L. and Mitchell, H. L.: Data assimilation using an ensemble Kalman filter technique, Monthly weather review, 126, 796–811, 1998.

Houtekamer, P. L. and Mitchell, H. L.: A sequential ensemble Kalman filter for atmospheric data assimilation, Monthly weather review, 129, 123–137, 2001.

Huber, P. J.: Robust estimation of a location parameter, in: Breakthroughs in statistics: Methodology and distribution, pp. 492–518, Springer, 1992.

Kageyama, M., Harrison, S. P., Kapsch, M. L., Löfverstrom, M., Lora, J. M., Mikolajewicz, U., Sherriff-Tadano, S., Vadsaria, T., Abe-Ouchi, A., Bouttes, N., Chandan, D., Gregoire, L. J., Ivanovic, R. F., Izumi, K., LeGrande, A. N., Lhardy, F., Lohmann, G., Morozova, P. A., Ohgaito, R., Paul, A., Peltier, W. R., Poulsen, C. J., Quiquet, A., Roche, D. M., Shi, X., Tierney, J. E., Valdes, P. J., Volodin, E., and Zhu, J.: The PMIP4 Last Glacial Maximum experiments: preliminary results and comparison with the PMIP3 simulations, Climate of the Past, 17, 1065–1089, https://doi.org/10.5194/cp-17-1065-2021, 2021.

https://doi.org/10.5194/egusphere-2026-1424
Preprint. Discussion started: 1 June 2026

Lei, L. and Anderson, J. L.: Comparisons of empirical localization techniques for serial ensemble Kalman filters in a simple atmospheric general circulation model, Monthly Weather Review, 142, 739–754, 2014a.

Lei, L. and Anderson, J. L.: Empirical localization of observations for serial ensemble Kalman filter data assimilation in an atmospheric general circulation model, Monthly Weather Review, 142, 1835–1851, 2014b.

Lenssen, N. J., Schmidt, G. A., Hansen, J. E., Menne, M. J., Persin, A., Ruedy, R., and Zyss, D.: Improvements in the GISTEMP uncertainty model, Journal of Geophysical Research: Atmospheres, 124, 6307–6326, 2019.

Liu, Z., Zhu, J., Rosenthal, Y., Zhang, X., Otto-Bliesner, B. L., Timmermann, A., Smith, R. S., Lohmann, G., Zheng, W., and Elison Timm, O.: The Holocene temperature conundrum, Proceedings of the National Academy of Sciences, 111, E3501–E3505, 2014.

Lorenz, E. N. et al.: Empirical orthogonal functions and statistical weather prediction, vol. 1, Massachusetts Institute of Technology, Department of Meteorology Cambridge, 1956.

Luo, G., Zeng, Y., Zhu, F., and Zhao, J.: Paleoclimate data assimilation with adaptive observation error inflation and adaptive localization, https://doi.org/https://doi.org/10.5281/zenodo.19015635, 2026.

Mann, M. E., Bradley, R. S., and Hughes, M. K.: Global-scale temperature patterns and climate forcing over the past six centuries, Nature, 392, 779–787, 1998.

Mann, M. E., Zhang, Z., Hughes, M. K., Bradley, R. S., Miller, S. K., Rutherford, S., and Ni, F.: Proxy-based reconstructions of hemispheric and global surface temperature variations over the past two millennia, Proceedings of the National Academy of Sciences, 105, 13 252–13 257, 2008.

Ménétrier, B., Montmerle, T., Michel, Y., and Berre, L.: Linear filtering of sample covariances for ensemble-based data assimilation. Part I: Optimality criteria and application to variance filtering and covariance localization, Monthly Weather Review, 143, 1622–1643, 2015a.

Ménétrier, B., Montmerle, T., Michel, Y., and Berre, L.: Linear filtering of sample covariances for ensemble-based data assimilation. Part II: Application to a convective-scale NWP model, Monthly Weather Review, 143, 1644–1664, 2015b.

Minamide, M. and Zhang, F.: Adaptive observation error inflation for assimilating all-sky satellite radiance, Monthly Weather Review, 145, 1063–1081, 2017.

Osman, M. B., Tierney, J. E., Zhu, J., Tardif, R., Hakim, G. J., King, J., and Poulsen, C. J.: Globally resolved surface temperatures since the Last Glacial Maximum, Nature, 599, 239–244, 2021.

PAGES 2k Consortium: A global multiproxy database for temperature reconstructions of the Common Era, Scientific Data, 4, 170 088, https://doi.org/10.1038/sdata.2017.88, 2017.

Parzen, E.: On estimation of a probability density function and mode, The annals of mathematical statistics, 33, 1065–1076, 1962.

Phipps, S. J., McGregor, H. V., Gergis, J., Gallant, A. J., Neukom, R., Stevenson, S., Ackerley, D., Brown, J. R., Fischer, M. J., and Van Ommen, T. D.: Paleoclimate data–model comparison and the role of climate forcings over the past 1500 years, Journal of Climate, 26, 6915–6936, 2013.

Sun, H., Lei, L., Liu, Z., Ning, L., and Tan, Z.-M.: An online paleoclimate data assimilation with a deep learning-based network, Journal of Advances in Modeling Earth Systems, 17, e2024MS004 675, 2025.

Tardif, R., Hakim, G. J., Perkins, W. A., Horlick, K. A., Erb, M. P., Emile-Geay, J., Anderson, D. M., Steig, E. J., and Noone, D.: Last Millennium Reanalysis with an expanded proxy database and seasonal proxy modeling, Climate of the Past, 15, 1251–1273, 2019.

Tingley, M. P., Craigmile, P. F., Haran, M., Li, B., Mannshardt, E., and Rajaratnam, B.: Piecing together the past: statistical insights into paleoclimatic reconstructions, Quaternary Science Reviews, 35, 1–22, 2012.

https://doi.org/10.5194/egusphere-2026-1424
Preprint. Discussion started: 1 June 2026

Vaccaro, A., Emile-Geay, J., Guillot, D., Verna, R., Morice, C., Kennedy, J., and Rajaratnam, B.: Climate field completion via Markov random fields: Application to the HadCRUT4. 6 temperature dataset, Journal of Climate, 34, 4169–4188, 2021.

Von Storch, H., Cubasch, U., Gonzalez-Rouco, J., Jones, J., Voss, R., Widmann, M., and Zorita, E.: Combining paleoclimatic evidence and GCMs by means of data assimilation through upscaling and nudging (DATUN), GKSS FORSCHUNGSZENTRUM GEESTHACHT GMBH-PUBLICATIONS-E, pp. 15–18, 2000.

Wang, J., Emile-Geay, J., Guillot, D., McKay, N. P., and Rajaratnam, B.: Fragility of reconstructed temperature patterns over the Common Era: Implications for model evaluation, Geophysical Research Letters, 42, 7162–7170, 2015.

Widmann, M., Goosse, H., van der Schrier, G., Schnur, R., and Barkmeijer, J.: Using data assimilation to study extratropical Northern Hemisphere climate over the last millennium, Climate of the Past, 6, 627–644, 2010.

Zeng, Y. and Janjić, T.: Study of conservation laws with the local ensemble transform kalman filter, Quart. J. Roy. Meteor. Soc., 699, 2359–2372, 2016.

Zhu, F., Emile-Geay, J., Anchukaitis, K. J., McKay, N. P., Stevenson, S., and Meng, Z.: A pseudoproxy emulation of the PAGES 2k database using a hierarchy of proxy system models, Scientific Data, 10, 624, 2023.

Zhu, F., Emile-Geay, J., Hakim, G. J., Guillot, D., Khider, D., Tardif, R., and Perkins, W. A.: cfr (v2024. 1.26): a Python package for climate field reconstruction, Geoscientific Model Development, 17, 3409–3431, 2024.